Spin dynamics study in layered van der Waals single-crystal Cr₂Ge₂Te₆

S. Khan,[1,*] C. W. Zollitsch,[1] D. M. Arroo,[1] H. Cheng,[2] I. Verzhbitskiy,[3] A. Sud,[1] Y. P. Feng,[3] G. Eda,[3] and H. Kurebayashi[1,†]

[1]*London Centre for Nanotechnology, University College London, London WC1H 0AH, United Kingdom*
[2]*Department of Physics, University of Science and Technology Beijing, Beijing 100083, China*
[3]*Department of Physics, National University of Singapore, 2 Science Drive 3, Singapore 117551*

We study the magnetization dynamics of a bulk single crystal Cr₂Ge₂Te₆ (CGT), by means of broadband ferromagnetic resonance (FMR), for temperatures from 60 K down to 2 K. We determine the Kittel relations of the fundamental FMR mode as a function of frequency and static magnetic field for the magnetocrystalline easy—and hard—axis. The uniaxial magnetocrystalline anisotropy constant is extracted and compared with the saturation magnetization, when normalized with their low temperature values. The ratios show a clear temperature dependence when plotted in the logarithmic scale, which departs from the predicted Callen-Callen power law fit of a straight line, where the scaling exponent n, $K_u(T) \propto [M_s(T)/M_s(2\ \text{K})]^n$, contradicts the expected value of 3 for uniaxial anisotropy. Additionally, the spectroscopic g factor for both the magnetic easy—and hard—axis exhibits a temperature dependence, with an inversion between 20 K and 30 K, suggesting an influence by orbital angular momentum. Finally, we qualitatively discuss the observation of multidomain resonance phenomena in the FMR spectras, at magnetic fields below the saturation magnetization.

I. INTRODUCTION

Two-dimensional (2D) van der Waals (vdWs) single crystals, belonging to the family of lamellar ternary chalcogenides (i.e., CGT and Cr₂Si₂Te₆) and chromium halides (i.e., CrI₃ and CrBr₃), have recently attracted a great deal of interest due to the presence of long range magnetic order in the 2D limit [1–4]. The presence of ferromagnetism in the 2D state has a potential to open new avenues in the field of spintronics leading to new magneto-optical and magnetoelectric applications [5,6]. Recent study of gate-tunable room temperature ferromagnetism in layered 2D Fe₃GeTe₂ [7] and the discovery of near room temperature ferromagnetism in the cleavable Fe₅GeTe₂ [8] have highlighted the significance that these layered vdWs systems can have for spintronics devices with room temperature applications. Thermal fluctuations in 2D systems at finite temperatures can restrain the long range magnetic order according to the Mermin-Wagner theorem [9], however due to the presence of large magnetocrystalline anisotropy in these layered systems the magnetic order remains dominant down to a few layers.

Chromium tellurogermanate, CGT, is a layered 2D ferromagnetic semiconductor with vdWs coupling between the adjacent layers. Bulk CGT has a trigonal crystal structure with the R$\bar{3}$ space group [10]. CGT has been a subject of vast experimental studies over the past few years. Gong *et al.* discovered the intrinsic ferromagnetism in atomic bilayers of CGT using the magneto-optical technique and showed significant control between paramagnetic to ferromagnetic transition temperature with very small magnetic fields [4]. For CGT with only few layers (≈3.5 nm thickness of crystalline flakes), Wang *et al.* demonstrated the control of magnetism by an electric field, showing a possibility for new applications in 2D vdWs magnets [11]. Liu *et al.* report an anisotropic magnetocaloric effect associated with the critical behavior of CGT and provide evidence of 2D Ising-like ferromagnetism, which is preserved in few-layer devices [12]. There still remains an ambiguity in the type of magnetic interaction in CGT, as experimentally, Heisenberg-like ferromagnetism is reported [4], but other reports looking at the critical exponents in CGT predict 2D Ising-like ferromagnetism [13,14].

CGT has been proposed as a potential substrate for topological insulators in order to realize the quantum anomalous Hall effect, and a large anomalous Hall effect in the bilayer structure of Bi₂Te₃ and CGT has been already observed [15]. To this point, there has been only one brief report of determination of the uniaxial magnetic anisotropy in CGT by ferromagnetic resonance (FMR) [16], while recent experiments rely on probing the sample by means of magneto-optical, magnetometry, and transport techniques. Understanding the magnetization dynamics by FMR is beneficial as it exactly measures the magnetic ground state [17], i.e., uniform-mode excitations of spin waves with $k \approx 0$. The FMR experiment allows us to determine the magnetic anisotropies in the system, the spectroscopic splitting g factor, and additionally it can provide information on the relative orbital contribution to the magnetic moment [18]. Therefore, it is significant to better understand the magnetization dynamics in bulk CGT in order to unfold the full potential of these layered vdWs systems in the field of spintronics.

In this paper, we report on a broadband FMR study in CGT in the temperature range of 60–2 K, with the external magnetic field applied along the in-plane (*ab*-plane) and out-of-plane (*c*-axis) orientations. The extracted value of the

*safe.khan.11@ucl.ac.uk
†h.kurebayashi@ucl.ac.uk

uniaxial magnetocrystalline anisotropy constant, K_u, is found to be temperature dependent. We find that the scaling of magnetic anisotropy constant and saturation magnetization as a function of temperature deviates from the theoretical prediction by the Callen-Callen power law. The determined g factor in CGT is found to be anisotropic for the different crystallographic directions. Finally, we observe a domain-mode resonance phenomenon below the saturation field. This indicates a presence of multiple domain structures in CGT.

II. EXPERIMENTAL DETAILS

CGT single-crystalline flakes were synthesized by the direct vapor transport (or flux) method. High-purity elemental Cr (99.9999% in chips), Ge (99.9999% in crystals), and Te (99.9999% in beads) were pre-mixed at molar ratio of 20:27:153 and sealed in the quartz ampule at high vacuum ($\approx 10^{-5}$ Torr). The ampule was loaded in the single-zone furnace, heated up to 1273 K with the rate of 2 K/min and left for two days. For a low-defect crystal growth, the furnace was set to slow cooling with the rate of 5 K/hour down to 673 K. Then, the furnace was turned off for natural cooling. The layered single-crystalline flakes were separated from the flux buildup and stored in the inert atmosphere of the glovebox. The bulk single crystals of CGT are not air sensitive, and it is also the case for our sample whereas it is different for a few layers of the CGT where the bilayer degrades after 90 mins of exposure to air [4].

Magnetization measurements were carried out at 2 K and 60 K with a vibrating sample magnetometer in a Quantum Design PPMS-14T, with measurements taken for both in-plane and out-of-plane applied magnetic fields. The Curie temperature of CGT is determined through heat capacity measurements carried out in the absence of any magnetic fields by thermal relaxation calorimetry in the PPMS [19].

A standard broadband FMR technique is used for the study of magnetization dynamics in CGT [20–22]. To employ a broadband oscillatory magnetic field to the sample, a silver plated copper co-planar waveguide (CPW) on a Rogers 4003c PCB, with a center conductor width of 1 mm and a gap of 0.5 mm, is used. The impedance matching of the microwave circuitry connected to the CPW is important for consideration when using it for FMR experiments, and it is carefully matched to 50 Ω [23]. The PCB is mounted inside a cooper sample box and features two SMP connectors, allowing the connection to the microwave circuitry. The sample box is attached to a probe, which is fitted inside a closed cycle helium flow cryostat, with a temperature range of 2–300 K. In addition, the cryostat is equipped with a rotation stage, allowing static magnetic field angle dependence measurements. The static magnetic field is generated by an electromagnet (Bruker ER073) which is able to produce a highly homogeneous field at the sample location.

We perform broadband microwave transmission experiments, using a vector network analyzer (VNA, Hewlett Packard). The microwave transmission S$_{21}$ is measured as a function of VNA frequency and static magnetic field. The FMR signature is identified by a strong microwave absorption, hence a reduction of transmission.
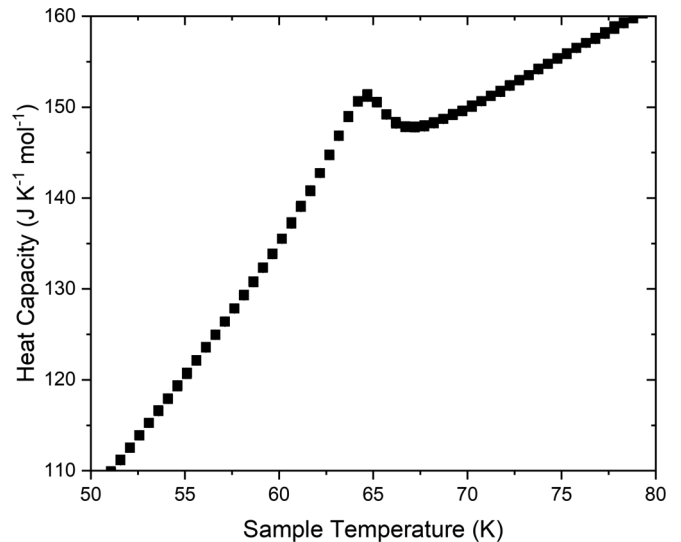

FIG. 1. Heat capacity of a CGT sample measured by thermal relaxation calorimetry. The anomaly in the heat capacity associated with the paramagnetic to ferromagnetic transition indicates a Curie temperature of 64.7 ± 0.5 K.

III. RESULTS AND DISCUSSION

The Curie temperature of the CGT sample is determined to be $T_c = 64.7 \pm 0.5$ K via a characteristic peak in the heat capacity associated with magnetic ordering (Fig. 1). The cusp in the heat capacity data as a function of sample temperature corresponds to collinear magnetic ordering in CGT, as reported elsewhere [14].

The magnetization of the CGT sample is measured below the Curie temperature for fields along the in-plane and out-of-plane directions, yielding respective saturation magnetizations of 2.68 ± 0.06 and 2.78 ± 0.06 μ_B per Cr atom at 2 K (Fig. 2). These values are close to the theoretically expected value of 3 μ_B per Cr atom [24], with the smaller value observed for the in-plane direction likely due to incomplete saturation at the maximum applied field of 5 T.

The broadband FMR, for externally applied magnetic fields along the in-plane and out-of-plane directions for 60 K, 30 K, and 2 K are shown in Fig. 3. The inset shows an exemplary experimental resonance spectra. The resonance is described by the derivation of the dynamic susceptibility from the Landau-Lifshitz and Gilbert equation, and hence it is analyzed by fitting a linear combination of symmetric and antisymmetric Lorentzian functions in order to determine the resonance field H_r (i.e., peak position) [25]. The frequency dependence of H_r exhibits the typical characteristic of magnetization dynamics in a ferromagnet with easy and hard magnetic axis. The easy axis in this case is along the c axis (out of plane), which shows a linear frequency dependence with a nonzero y intercept corresponding to the anisotropy field. The ab-plane (in-plane) resonance spectra shows a nonlinear frequency dependence with the x intercept increasing in value as the temperature is decreased from 60 K to 2 K, exhibiting an increase in the uniaxial magnetocrystalline anisotropy. The dotted lines show the expected resonance spectra of a uniform ferromagnetic resonance in single domain crystals. An important observation
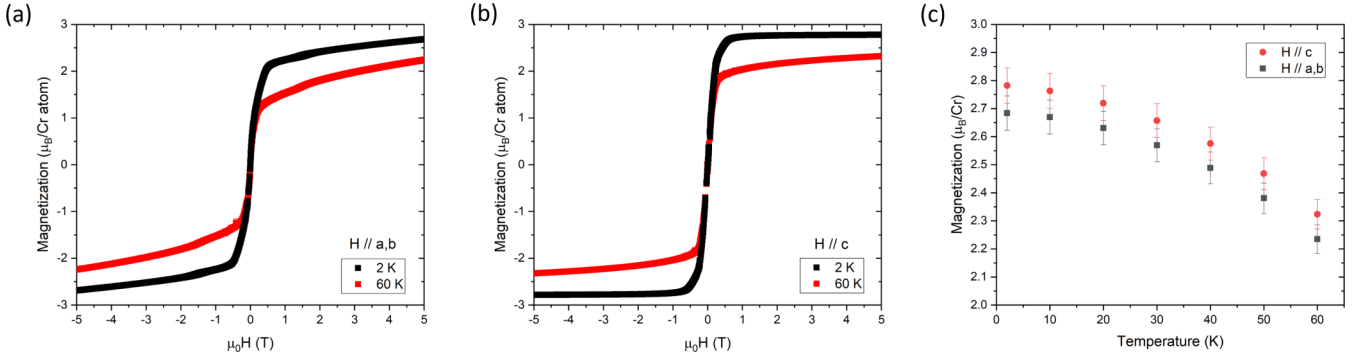
FIG. 2. Magnetization data for CGT measured via vibrating sample magnetometry carried out at temperatures from 2 K to 60 K. (a) Magnetization curves with the field applied along the in-plane direction. (b) Magnetization curves with the field applied along the out-of-plane direction. (c) Magnetization with an applied field of 5 T as a function of temperature.

in the extracted FMR Kittel relations is the difference in slope for in-plane and out-of-plane orientations. Additionally, the slope for the two orientations shows a temperature dependence. This suggests that the spectroscopic g factor is not isotropic for CGT (discussed in more detail below).

In the following we discuss the fitting equations derived by the Smit-Beljers-Suhl approach [26,27], which are used to fit the experimental data along the in-plane and out-of-plane directions in Fig. 3. The spatial distribution of the free energy density F is probed by the FMR experiment. The free energy density for the CGT system excluding exchange energy (in-plane dimensions of 2×1.5 mm and thickness of 0.3 mm, i.e., in the out-of-plane direction) reads

$$F = -\mathbf{M} \cdot \mathbf{H} + 2\pi (\mathbf{M} \cdot \mathbf{n})^2 - K_u \left(\mathbf{M} \cdot \frac{\mathbf{z}}{M_s} \right)^2, \quad (1)$$
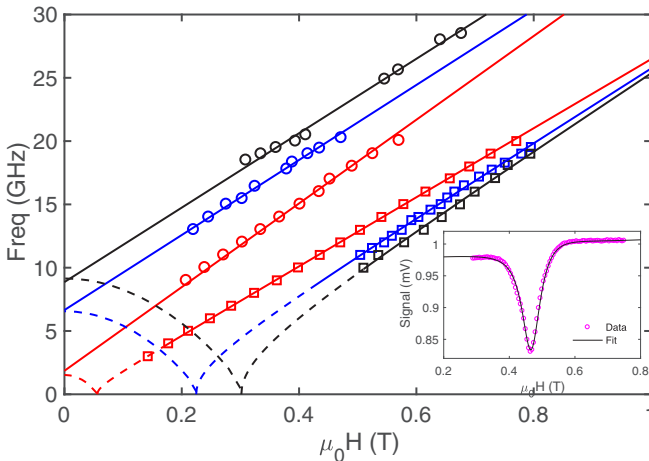

FIG. 3. The inset shows the experimental resonance spectra with a Lorentzian line shape (black line). Main plot shows frequency dependence of resonance field at 60 K (red), 30 K (blue), and 2 K (black), along the in-plane (squares data points) and out-of-plane (circle data points) orientations. The solid lines represent the Kittel fitting for both orientations giving straight line fit along the c axis [fitted with Eq. (8)] and square-root dependence along the ab plane [fitted with Eq. (7)] i.e., easy and hard axis, respectively. The dotted lines along in-plane orientation show an expected spectrum of frequency dependence for a single domain case.

where $\mathbf{H}$ and $\mathbf{M}$ are the external magnetic field and magnetization vectors, respectively. The first term in Eq. (1) is the Zeeman energy, the second term is the demagnetization energy, and the third term is the uniaxial magnetic anisotropy term, with K_u, the magnetocrystalline anisotropy constant, M_s, the saturation magnetization, and $\mathbf{n}$ and $\mathbf{z}$ are the unit vectors normal to the surface of the sample and orientated along the easy axis (c axis), respectively. $\mathbf{H}$ and $\mathbf{M}$ are then written as

$$\mathbf{H} = H \begin{pmatrix} \sin(\theta_H) \cos(\phi_H) \\ \sin(\theta_H) \sin(\phi_H) \\ \cos(\theta_H) \end{pmatrix}, \quad (2)$$

$$\mathbf{M} = M_s \begin{pmatrix} \sin(\theta_M) \cos(\phi_M) \\ \sin(\theta_M) \sin(\phi_M) \\ \cos(\theta_M) \end{pmatrix}, \quad (3)$$

where $\theta_{H/M}$ and $\phi_{H/M}$ are the polar (accounted from normal to the rectangular sample platelet ab plane) and azimuthal (in-plane) angles, respectively. The double derivatives approach of the magnetic free energy with respect to the polar and azimuthal angles [i.e., substituting equations (1), (2), and (3) into Eq. (4)] is then used to analytically calculate the resonance frequency [26,27], $\omega = 2\pi f$, as

$$\left(\frac{\omega}{\gamma} \right)^2 = \frac{1}{M_s \sin(\theta_M)} \left[\frac{\partial^2 F}{\partial \theta_M^2} \frac{\partial^2 F}{\partial \phi_M^2} - \left(\frac{\partial^2 F}{\partial \theta_M \partial \phi_M} \right)^2 \right], \quad (4)$$

where γ is the gyromagnetic ratio. The azimuthal angles in the CGT system [i.e., in Eqs. (2) and (3)] can be set to $\phi_{H/M} = 0$, as the in-plane magnetocrystalline anisotropy energy is negligible. Solving for the perpendicular anisotropy case ($\mathbf{n} = \mathbf{z}$, along the easy axis, i.e., parallel to the out-of-plane c axis), one arrives at the general Kittel relation for arbitrary polar angles of the external magnetic field with respect to the easy axis of the magnetization, which reads

$$\left(\frac{\omega}{\gamma} \right)^2 = [H_r \cos(\theta_H - \theta_M) - 4\pi M_{\text{eff}} \cos^2(\theta_M)]$$
$$\times [H_r \cos(\theta_H - \theta_M) - 4\pi M_{\text{eff}} \cos(2\theta_M)], \quad (5)$$

where H_r is the ferromagnetic resonance field, $4\pi M_{\text{eff}} = 4\pi M_s - H_u$ is the effective demagnetization field and $H_u = 2K_u/\mu_0 M_s$, the perpendicular anisotropy field, and since the trigonal CGT system with a point group of $\bar{3}$ lacks the C_4 symmetry in the unit cell, the fourth order anisotropy constant

is not taken into account in the fitting of the FMR spectra, and the higher order anisotropy terms have not been considered in other studies [28–30]. The angular dependence of the resonance frequency from the in-plane to out-of-plane axis also does not show any fourfold dependence (Fig. S5 in the Supplemental Material) [24]. On resonance, the values for θ_M can be determined by the condition $\partial F/\partial \theta_M = 0$ and are given by

$$\sin(2\theta_M) = \frac{2H_r}{4\pi M_s - H_u}\sin(\theta_M - \theta_H) \ . \tag{6}$$

The Kittel equations for the in-plane ($\parallel$) and perpendicular ($\perp$) orientations can be determined by setting $\theta_M = \theta_H$ in a saturated state and are given by

$$\omega_{(\parallel)} = \gamma\sqrt{H_r(H_r + 4\pi M_{eff})} \ , \tag{7}$$

$$\omega_{(\perp)} = \gamma(H_r - 4\pi M_{eff}) \ . \tag{8}$$

The above equations are used to fit the in-plane and out-of-plane FMR data in Fig. 3, with spectroscopic g factor (contained in $\gamma = g\mu_B/\hbar$) and M_{eff} as fitting parameters. The extracted parameters from the Kittel relations are also used to calculate the dependence of the resonance frequency as a function of externally applied magnetic field, and the angle-dependent resonance spectrum together with the calculated curves is shown in the Supplemental Material [24].

The temperature dependence of the out-of-plane uniaxial magnetocrystalline anisotropy constant, K_u, is shown in Fig. 4(a). This was determined from the least-square fitting of Eqs. (7) and (8) to the frequency-dependent FMR spectra. A positive sign convention is used, where $K_u > 0$ favors perpendicular magnetic anisotropy. K_u is found to be in the range of $(0.77 - 3.95) \times 10^5$ erg/cm³ from 2 K to 60 K, which confirms that the magnetic easy axis in CGT is along the c axis as seen by the magnetometry data and previous experimental observations [10,16]. The reported magnetocrystalline anisotropy energies for other similar layered 2D magnets are $K_u = 1.46 \times 10^7$ erg/cm³ at 4 K and $K_u = 3.1 \times 10^6$ erg/cm³ at 1.5 K, for Fe_3GeTe_2 [28] and CrI_3 [29], respectively. CGT is found to be less anisotropic than these systems whereas the ferromagnetic T_c of CGT is close to that of CrI_3 ($\sim$61 K) and Fe_3GeTe_2 possesses high transition temperature ($\sim$223 K). At 2 K, the anisotropy energy value corresponds to 0.24 meV per unit cell of CGT, which is six times smaller than the value, 1.4 meV per unit cell, obtained from the DFT calculations [24] (see also Refs. [31–40] therein used for the DFT calculations). The difference in the experimental and calculated magnetic anisotropy energy can arise as (i) the DFT calculation is done at 0 K, (ii) the structure model used in the calculation is considered to be a defect-free system (the unit cell considered for DFT calculations can be seen in the Supplemental Material [24]).

In Fig. 4(b), the reduced anisotropy constant, $K_u(T)/K_u(2\ \text{K})$, and the reduced magnetization, $M_s(T)/M_s(2\ \text{K})$, at different temperatures are shown for the CGT single crystal. The theory of the temperature dependence of magnetic anisotropies was developed by Callen and Callen, and others [42–44]. It predicts that the magnetocrystalline anisotropy constant as a function of temperature for uniaxial and cubic systems distinctly differs
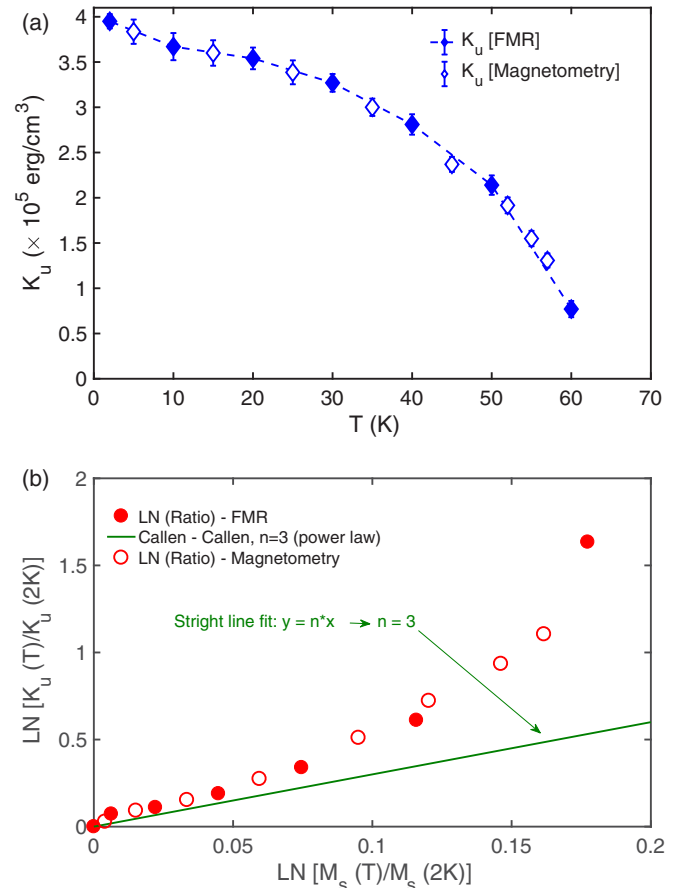

FIG. 4. (a) Temperature dependence of uniaxial magnetocrystalline anisotropy constant K_u, where the filled points are extracted from the FMR data as discussed in the main text and the nonfilled points are extracted from the magnetometry measurements [41]. (b) The ratio $K_u(T)/K_u(2\ \text{K})$ is compared with the ratio $[M_s(T)/M_s(2\ \text{K})]$ in the absolute value of the logarithm scale. A solid line with the exponent, $n = 3$, is plotted to highlight that the experimental data does not follow the Callen-Callen behavior.

depending on the crystal symmetry and on the degree of correlations between the direction of neighboring spins. The famous Callen-Callen power law based on the single-ion anisotropy model relates the temperature dependence of K_u to M_s in the low temperature limit (T $\ll$ T_c) as

$$\frac{K_u(T)}{K_u(0)} = \left[\frac{M_s(T)}{M_s(0)}\right]^n \ , \tag{9}$$

where the exponent, $n = l(l+1)/2$, depends on the crystal symmetry and degree of correlations between adjacent spins, and l being the order of spherical harmonics, and it describes the angular dependence of the local anisotropy. In the case of uniaxial anisotropy, the exponent is predicted to be $n = 3$ and it suggests a single-ion origin of magnetic anisotropy.

An unexpected behavior of the scaling between the temperature dependence of the anisotropy constant and magnetization is found in hexagonal CGT. This can be seen in Fig. 4(b), where the experimental data departs from the trend of a straight line (plotted in logarithmic scale) with a slope of $n = 3$, predicted by the Callen-Callen power law

for uniaxial systems. In simple ferromagnetic systems such as ultrathin Fe films [45], the Callen-Callen power law for uniaxial anisotropy has been experimentally verified, across the whole temperature range below T_c, with an exponent $n = 2.9$, and it is considered as a good model for ferromagnets with localized moments. In the past, deviations from the expected scaling exponent of $n = 3$ have been reported in complex systems containing a nonmagnetic material with a large spin-orbit coupling, which can contribute to magnetic anisotropy without having a significant effect on other magnetic properties [46–48]. In highly anisotropic barium ferrite systems, K_u was found to be linearly proportional to M_s, clearly inconsistent from the theoretical predictions [49]. The departure from the Callen-Callen theory for these reported systems is suggested due to the violation of simple assumptions considered in the theory [50], (i) magnetization origin in the material coming from single ions with localized magnetic moments, (ii) spin-orbit coupling being regarded as a small perturbation to the exchange coupling, and (iii) temperature dependence of anisotropy and magnetization having the same origin. Recent first principles calculations in CGT predict the interplay between single-ion anisotropy and Kitaev interaction [51]. They are found to be induced by the off-site spin-orbit coupling of the heavy ligand, i.e., Te atoms. Another recent study [52], investigating the origin of magnetic anisotropy in layered ferromagnetic Cr compounds, suggests that an additional magnetic exchange anisotropy induced by the spin-orbit coupling from the ligand p orbital through superexchange mechanism plays a crucial role in determining the magnetocrystalline anisotropy in CGT and other layered systems such as CrI$_3$ and CrSiTe$_3$. Hence, CGT is a complex magnetic system with no simple correlation between the thermal behavior of anisotropy and magnetization.

The temperature dependence of the spectroscopic g factor for the in-plane (*ab*-plane) and out-of-plane (*c*-axis) orientations, can be seen in Fig. 5. There is contrasting behavior in the temperature dependence of the g factor, where g increases with decreasing temperature in the in-plane (hard-axis) direction, and it decreases in the out-of-plane (easy-axis) direction as the temperature decreases. At 2 K, $g_\parallel = 2.18 \pm 0.02$ (*ab* plane) and $g_\perp = 2.10 \pm 0.01$ (*c* axis), indicating that the g factor is anisotropic in CGT and shows a crossing between 20 K and 30 K. The g factor is determined by extracting the proportionality of the gyromagnetic ratio in Eqs. (7) and (8), given by $\gamma = g\mu_B/\hbar$, where μ_B is the Bohr magneton and $\hbar$ is the reduced Plancks constant. Determining a value of g is important since one can find the relative spin and orbital moments of a material by using the well-known relation [53]

$$\frac{\mu_L}{\mu_S} = \frac{g - 2}{2} \quad , \qquad (10)$$

where μ_L is the orbital moment per spin and $\mu_S = \mu_B$ is the spin moment. The deviation of the spectroscopic factor from the electron's g factor of $g = 2$ suggests an orbital contribution to the magnetization [54]. The g value of the free electron case is considered in systems where the orbital moment is assumed to be nearly completely quenched due to the high symmetry of the bulk crystals, and hence magnetism in such systems is described in terms of pure spin magnetism. The nonspherical charge distribution in the d shells can prevent the complete
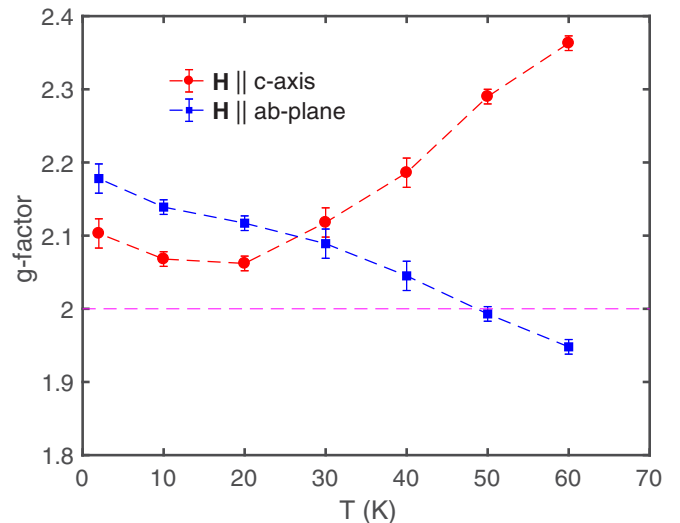

FIG. 5. Temperature dependence of the spectroscopic g factor with external magnetic field along the c axis (easy axis, red circles) and the *ab* plane (hard axis, blue squares). The dashed horizontal line (magenta) at $g = 2$ indicates a case of pure spin magnetism where the orbital moment is completely quenched.

quenching of the orbital momentum [55], i.e., $L_z \neq 0$. An orbital moment of 8% and 5% for μ_L/μ_S along the in-plane and out-of-plane orientations, respectively, is found in CGT at 2 K. The small orbital moment anisotropy could be explained by the presence of the spin-orbit interaction from the d orbitals of the Cr atoms as well as the off-site spin-orbit coupling of p orbitals of Te atoms [24], giving g a tensor character, i.e., dependence on the crystallographic directions. The g-factor extraction from the FMR experiment here only gives a relative insight into the orbital moment contribution to the magnetism in CGT. One can determine the orbital moment μ_L and its anisotropy from the x-ray magnetic circular dichroism (XMCD) experiments at synchrotron facilities in order to further improve the understanding of orbital magnetism in these layered van der Waals magnetic systems [56–58]. In fact, the study referenced previously [52] looking into the origin of magnetic anisotropy in layered 2D systems also carries out an initial XMCD investigation of Cr $L_{2,3}$ edge in CGT at 20 K. They report a sizable anisotropy in the orbital angular momentum (i.e., related to the orbital moment), where $L_c = -0.045$, $L_{ab} = -0.052$, and $\Delta L = 0.007$. This work complements our results of the g-factor anisotropy obtained in the FMR experiment, where a deviation from $g = 2$ confirms the presence of orbital angular momentum in CGT.

In Fig. 6, the temperature evolution from 60 K to 2 K of the frequency-dependent FMR spectrum in the in-plane (hard-axis) orientation is shown. The red arrows indicate the saturation field points for the CGT system, where a transition from the multidomain magnetic states to a single domain state occurs in the sample [59]. At 60 K, there is no sign of domain-mode resonance but as the temperature decreases, the strength of the perpendicular uniaxial magnetic anisotropy increases, and the multiple domain-mode resonances (dotted white lines) appear. Qualitatively, this shows the presence of multidomain structures in bulk CGT [60]. The FMR setup used in this
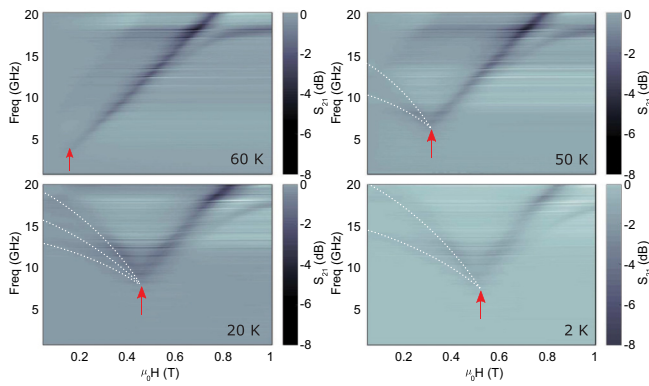
FIG. 6. Temperature evolution of the frequency-dependent ferromagnetic resonance spectra (in-plane orientation) from 60 K to 2 K. The red arrow indicates the saturation field point in the system where the system goes from multidomain to single domain state. The dotted white lines do not represent any fittings and are used only for guidance.

experiment is sensitive to observe the resonance of these domain structures. The minimum feature of the resonance frequency (red arrow) increases with decreasing temperature. This type of feature is markedly different for samples with a single magnetic domain state [61], where the frequency-dependent resonance spectra has an *x* intercept along the hard axis of magnetization.

The *M-H* curves in Figs. 2(a) and 2(b) show no hysteresis behavior, but this does not reflect signatures of a single domain system below the saturation state for CGT. The remanent magnetization at zero external magnetic field does not have any net magnetization, indicating magnetic moment cancellation due to multidomain states with up-and-down flux closures. This seems to be common for layered van der Waals magnets, i.e., exhibiting a soft magnetic behavior of a linear *M-H* curve before saturation [62,63]. The experimental evidence of the presence of multiple magnetic domain structures in bulk CGT along the in-plane sample orientation has been confirmed recently using magnetic force microscopy [64]. The observed domain structures were classified with different symmetry types and showed an evolution from one symmetry type to another as a function of both temperature and external magnetic field. This reaffirms that the features seen in the magnetization dynamics experiment below the saturation field (Fig. 6) corresponds to dynamics of multiple magnetic domain structures. Although the presence of multidomains is realized by the FMR experiment, it is not possible to obtain the symmetry and type of structures for these domains by a resonance

experiment alone. Hence, one has to be careful in extracting any magnetic parameters in the bulk layered CGT system at low magnetic fields as a small dynamic demagnetizing field can exist from the interaction of different magnetic domains with each other and also with that of domain wall boundaries.

IV. CONCLUSION

In summary, we studied the FMR behavior in bulk two-dimensional CGT. In particular, broadband FMR experiments were performed within the temperature range of 60–2 K with external magnetic fields along the in-plane and out-of-plane orientations. Additionally, the angular dependence of the FMR spectra was examined. We focused on the temperature dependence of the magnetic anisotropy energy, spectroscopic *g* factor, and the multidomain resonance features (observed below the saturation fields along the *ab* plane). A uniaxial perpendicular magnetic anisotropy is found with the easy axis parallel to the *c* axis (out of plane). The scaling of the normalized magnetocrystalline anisotropy constant and saturation magnetization showed a deviation from the theoretically predicted Callen-Callen power law. The presence of spin orbit coupling from *d* orbitals of Cr atoms and an offsite spin orbit coupling from p orbitals of the ligand Te atoms can be a contributing factor to this contradicting behavior of power law dependence of magnetic anisotropy to magnetization. The obtained *g* factor showed an anisotropic response, i.e., a crystallographic dependence, and at 2 K it was found to be $g_\parallel = 2.18 \pm 0.02$ (*ab* plane) and $g_\perp = 2.10 \pm 0.01$ (*c* axis). The determined *g*-factor values are greater than 2, again, indicating that the orbital magnetism plays an important role in bulk CGT when considering magnetic interactions in this system. A small anisotropy in the orbital magnetic moment relative to the spin moment is found, and a detailed x-ray magnetic circular dichroism study could give further insight into the orbital moment anisotropy. Finally, the presence of multidomain structures is qualitatively confirmed as domain-mode resonance phenomena are observed along the *ab*-plane (in-plane) orientation.

[1] B. Liu, Y. Zou, L. Zhang, S. Zhou, Z. Wang, W. Wang, Z. Qu, and Y. Zhang, Sci. Rep. **6**, 33873 (2016).

[2] Z. Wang, I. Gutiérrez-Lezama, N. Ubrig, M. Kroner, M. Gibertini, T. Taniguchi, K. Watanabe, A. Imamoğlu, E. Giannini, and A. F. Morpurgo, Nat. Commun. **9**, 2516 (2018).

[3] N. Richter, D. Weber, F. Martin, N. Singh, U. Schwingenschlögl, B. V. Lotsch, and M. Kläui, Phys. Rev. Materials **2**, 024004 (2018).

[4] C. Gong, L. Li, Z. Li, H. Ji, A. Stern, Y. Xia, T. Cao, W. Bao, C. Wang, Y. Wang, S. Louie *et al.*, Nature (London) **546**, 265 (2017).

[5] C. Cardoso, D. Soriano, N. García-Martínez, and J. Fernández-Rossier, Phys. Rev. Lett. **121**, 067701 (2018).

[6] Y. Fang, S. Wu, Z.-Z. Zhu, and G.-Y. Guo, Phys. Rev. B **98**, 125416 (2018).

[7] Y. Deng, Y. Yu, Y. Song, J. Zhang, N. Z. Wang, Z. Sun, Y. Yi, Y. Z. Wu, S. Wu, J. Zhu *et al.*, Nature (London) **563**, 94 (2018).

[8] A. F. May, D. Ovchinnikov, Q. Zheng, R. Hermann, S. Calder, B. Huang, Z. Fei, Y. Liu, X. Xu, and M. A. McGuire, ACS nano **13**, 4436 (2019).

[9] N. Mermin, Phys. Rev. Lett. **17**, 1133 (1966).

[10] Z. Lin, M. Lohmann, C. Tang, J. Li, W. Xing, J. Zhong, S. Jia, W. Han, and J. Shi, Phys. Rev. Materials **2**, 051004(R) (2018).

[11] Z. Wang, T. Zhang, M. Ding, B. Dong, Y. Li, M. Chen, X. Li, J. Huang, H. Wang, X. Zhao *et al.*, Nat. Nanotechnol. **13**, 554 (2018).

[12] Y. Liu and C. Petrovic, Phys. Rev. Materials **3**, 014001 (2019).

[13] Y. Liu and C. Petrovic, Phys. Rev. B **96**, 054406 (2017).

[14] W. Liu, Y. Dai, Y.-E. Yang, J. Fan, L. Pi, L. Zhang, and Y. Zhang, Phys. Rev. B **98**, 214420 (2018).

[15] L. Alegria, H. Ji, N. Yao, J. Clarke, R. Cava, and J. Petta, Appl. Phys. Lett. **105**, 053512 (2014).

[16] X. Zhang, Y. Zhao, Q. Song, S. Jia, J. Shi, and W. Han, Jpn. J. Appl. Phys. **55**, 033001 (2016).

[17] A. N. Anisimov, M. Farle, P. Poulopoulos, W. Platow, K. Baberschke, P. Isberg, R. Wäppling, A. Niklasson, and O. Eriksson, Phys. Rev. Lett. **82**, 2390 (1999).

[18] M. Farle, Rep. Prog. Phys. **61**, 755 (1998).

[19] J. Lashley, M. Hundley, A. Migliori, J. Sarrao, P. Pagliuso, T. Darling, M. Jaime, J. Cooley, W. Hults, L. Morales *et al.*, Cryogenics **43**, 369 (2003).

[20] S. He and C. Panagopoulos, Rev. Sci. Instrum. **87**, 043110 (2016).

[21] C. Bilzer, T. Devolder, P. Crozat, C. Chappert, S. Cardoso, and P. Freitas, J. Appl. Phys. **101**, 074505 (2007).

[22] E. Montoya, T. McKinnon, A. Zamani, E. Girt, and B. Heinrich, J. Magn. Magn. Mater. **356**, 12 (2014).

[23] D. M. Pozar, *Microwave Engineering* (John Wiley & Sons, Hoboken, NJ, 2009).

[24] See Supplemental Material at http://link.aps.org/supplemental/10.1103/PhysRevB.100.134437 for the theoretical DFT magnetic anisotropy energy calculations, saturation magnetization correction procedure, and the angle-dependent FMR results.

[25] Z. Celinski, K. Urquhart, and B. Heinrich, J. Magn. Magn. Mater. **166**, 6 (1997).

[26] J. Smit, Philips Res. Rep. **10**, 113 (1955).

[27] H. Suhl, Phys. Rev. **97**, 555 (1955).

[28] N. León-Brito, E. D. Bauer, F. Ronning, J. D. Thompson, and R. Movshovich, J. Appl. Phys. **120**, 083903 (2016).

[29] J. Dillon, Jr. and C. Olson, J. Appl. Phys. **36**, 1259 (1965).

[30] J. Zeisner, A. Alfonsov, S. Selter, S. Aswartham, M. P. Ghimire, M. Richter, J. van den Brink, B. Büchner, and V. Kataev, Phys. Rev. B **99**, 165109 (2019).

[31] Y. Sun, R. Xiao, G. Lin, R. Zhang, L. Ling, Z. Ma, X. Luo, W. Lu, Y. Sun, and Z. Sheng, Appl. Phys. Lett. **112**, 072409 (2018).

[32] S. Grimme, J. Comput. Chem. **27**, 1787 (2006).

[33] H. Takayama, K.-P. Bohnen, and P. Fulde, Phys. Rev. B **14**, 2287 (1976).

[34] G. H. O. Daalderop, P. J. Kelly, and M. F. H. Schuurmans, Phys. Rev. B **41**, 11919 (1990).

[35] D.-S. Wang, R. Wu, and A. Freeman, Phys. Rev. B **47**, 14932 (1993).

[36] P. E. Blöchl, Phys. Rev. B **50**, 17953 (1994).

[37] A. Liechtenstein, V. Anisimov, and J. Zaanen, Phys. Rev. B **52**, R5467(R) (1995).

[38] G. Kresse and J. Furthmüller, Phys. Rev. B **54**, 11169 (1996).

[39] Y. F. Li, W. Wang, W. Guo, C. Y. Gu, H. Y. Sun, L. He, J. Zhou, Z. B. Gu, Y. F. Nie, and X. Q. Pan, Phys. Rev. B **98**, 125127 (2018).

[40] J. P. Perdew, K. Burke, and M. Ernzerhof, Phys. Rev. Lett. **77**, 3865 (1996).

[41] F. Yang, C. Chien, E. Ferrari, X. Li, G. Xiao, and A. Gupta, Appl. Phys. Lett. **77**, 286 (2000).

[42] J. H. van Vleck, Phys. Rev. **52**, 1178 (1937).

[43] C. Zener, Phys. Rev. **96**, 1335 (1954).

[44] H. B. Callen and E. Callen, J. Phys. Chem. Solids **27**, 1271 (1966).

[45] K. Zakeri, T. Kebe, J. Lindner, and M. Farle, Phys. Rev. B **73**, 052405 (2006).

[46] R. Skomski, A. Kashyap, and D. J. Sellmyer, IEEE Trans. Magn. **39**, 2917 (2003).

[47] O. N. Mryasov, U. Nowak, K. Y. Guslienko, and R. W. Chantrell, Europhys. Lett. **69**, 805 (2005).

[48] A. Truong, A. O. Watanabe, T. Sekiguchi, P. A. Mortemousque, T. Sato, K. Ando, and K. M. Itoh, Phys. Rev. B **90**, 224415 (2014).

[49] J. Wang, F. Zhao, W. Wu, and G.-M. Zhao, J. Appl. Phys. **110**, 096107 (2011).

[50] B. K. Chatterjee, C. Ghosh, and K. Chattopadhyay, J. Appl. Phys. **116**, 153904 (2014).

[51] C. Xu, J. Feng, H. Xiang, and L. Bellaiche, npj Comput. Mater. **4**, 57 (2018).

[52] D.-H. Kim, K. Kim, K.-T. Ko, J. Seo, J. S. Kim, T.-H. Jang, Y. Kim, J.-Y. Kim, S.-W. Cheong, and J.-H. Park, Phys. Rev. Lett. **122**, 207201 (2019).

[53] C. Kittel, Phys. Rev. **76**, 743 (1949).

[54] J. M. Shaw, H. T. Nembach, T. J. Silva, and C. T. Boone, J. Appl. Phys. **114**, 243906 (2013).

[55] K. Baberschke, *Band-Ferromagnetism* (Springer, Berlin, Germany, 2001), pp. 27–45.

[56] B. B. Thole, G. Van der Laan, and G. A. Sawatzky, Phys. Rev. Lett. **55**, 2086 (1985).

[57] M. Altarelli, Phys. Rev. B **47**, 597 (1993).

[58] A. Frisk, L. B. Duffy, S. Zhang, G. van der Laan, and T. Hesjedal, Mater. Lett. **232**, 5 (2018).

[59] B. Lührmann, H. Dötsch, and S. Sure, Appl. Phys. A **57**, 553 (1993).

[60] M. Sigal, Phys. Status Solidi A **42**, 775 (1977).

[61] K. Zakeri, T. Kebe, J. Lindner, and M. Farle, J. Magn. Magn. Mater. **299**, L1 (2006).

[62] M. A. McGuire, G. Clark, K. Santosh, W. M. Chance, G. E. Jellison, Jr., V. R. Cooper, X. Xu, and B. C. Sales, Phys. Rev. Materials **1**, 014001 (2017).

[63] M. A. McGuire, H. Dixit, V. R. Cooper, and B. C. Sales, Chem. Mater. **27**, 612 (2015).

[64] T. Guo, Z. Ma, Y. Hou, Z. Sheng, and Q. Lu, arXiv:1803.06113.